IEEE Instrumentation and Measurement
Technology Conference
Anchorage, AK, USA, 21–23 May 2002

Modelling, calibration and rendition of colour logarithmic CMOS image sensors

Dileepan Joseph and Steve Collins
Engineering Science, University of Oxford, OX1 3PJ, United Kingdom
Phone +44 1865 273805, Fax +44 1865 273905, Email *mcad@robots.ox.ac.uk*

***Abstract** – Logarithmic CMOS image sensors encode a high dynamic range scene in a manner that roughly approximates human perception whereas linear sensors with equivalent quantisation suffer from saturation or loss of detail. Moreover, the continuous response of logarithmic pixels permit high frame rates and random access, features that are useful in motion detection. This paper describes how to model, calibrate and render pixel responses from a colour logarithmic sensor into a standard colour space. The work unifies colour theory in conventional linear sensors and fixed pattern noise theory in monochromatic logarithmic sensors. Experiments with a Fuga 15RGB sensor demonstrate calibration and rendition using a Macbeth chart and neutral density filters. Colour rendition of the sensor with an empirical model, tested over three decades of dynamic range, competes with conventional digital cameras, tested over 1.5 decades. Photodiode leakage currents complicate modelling and calibration and degrade rendition in dim lighting.*

***Keywords** – Logarithmic pixels, colour rendition, fixed pattern noise.*

I. INTRODUCTION

CMOS image sensors are displacing CCD sensors for several reasons, such as the integration of signal processing with image sensing on one die and the economies of scale available in the CMOS industry [1]. Research on CMOS imaging includes the development of sensors to capture high dynamic range scenes, where illuminances and reflectances span several decades, without saturation or loss of perceptible detail [2]. Conventional linear sensors adapt over a high dynamic range, preserving detail, but display saturated patches of black or white when presented with the whole range at once. Increasing the number of bits in the analogue-to-digital converter to extend the dynamic range of these sensors poses difficulties. Too many bits are needed, especially at video rates, and most of these are wasted as human perception has less absolute sensitivity to bright illuminances than to dim ones [3].

For reasons of high dynamic range coupled with high frame rate (and random accessibility of pixels), the automotive industry sees logarithmic sensors as a useful technology to help automate traffic supervision and improve road safety [4]. Human perception roughly approximates Weber's law, which says that the threshold to sense a difference between the illuminance of a fixation point and its surroundings is a fraction of the surrounding illuminance [3]. When illuminances are encoded by a logarithmic sensor, such a law makes the threshold for sensitivity constant, ideal for quantisation. Instead of integrating charge over discrete periods of time, logarithmic sensors convert incident light continuously into a current, which means that an image is available at virtually any moment. Studies with pulsed lasers have shown a pixel bandwidth of 100 kHz, at normal light levels, that increases with illumination [5]. In practice, the speed of the readout circuit limits the frame rate.

Applications involving safety require a robust technology. One problem with logarithmic sensors is fixed pattern noise (FPN), a substantial but predictable error that appears in an image due to natural variations of device parameters from pixel to pixel [6]. While FPN correction is necessary to make logarithmic sensors useful, the accurate rendition of scenes on display devices by estimation of real world stimuli from pixel responses is also important. Rendition is more important with colour images because the eye is more sensitive to chromatic errors than to intensity errors [3]. Much has been published about colour rendition in linear sensors but little has been written on rendition in colour logarithmic sensors, the subject of this paper.

Section II unites colour theory in linear sensors with monochromatic theory in logarithmic sensors to model colour sensation in logarithmic sensors. Section III describes a procedure to calibrate this model and Section IV outlines a method to render the response of a calibrated sensor into a standard colour space. Section V demonstrates calibration and rendition with a Fuga 15RGB logarithmic sensor, a colour version of the Fuga 15d developed at IMEC [7], and compares colour rendition of the sensor to that of conventional digital cameras.

II. MODELLING

A colour image sensor is made by inserting colour filters in the path of light rays before they form an image on a monochromatic sensor [8]. Corresponding to human colour vision, three filters are needed, selective to the red (R), green (G) and blue (B) regions of the spectrum. Multi-sensor imagers use prisms with special coatings to split and filter an image into three images, which are captured by separate sensors and combined to produce a single image. Single-sensor imagers have a pattern of red, green and blue filters overlaid upon pixels. Though each pixel is selective to one colour, its neighbours are selective to the others. By interpolating pixel responses, a red, green and blue response may be estimated for each pixel at a loss of spatial resolution. As multi-sensor imagers obey a similar theory, the rest of this paper discusses only single-sensor imagers.

0-7803-7218-2/02/$10.00 '2002 IEEE

A colour filter on a pixel modifies the spectral composition of incident light prior to absorption by the photodiode in the pixel. The photodiode absorbs the filtered light to varying degrees as a function of wavelength λ. Even attenuation in the lens of the camera is wavelength dependent. Equation (1) combines the spectral attenuations of the lens $g_L(\lambda)$, colour filter $g_k(\lambda)$, with $k \in \{R, G, B\}$, and photodiode $g_P(\lambda)$ into one function $f_k(\lambda)$ [8]. Equation (2) uses $f_k(\lambda)$ to model the photocurrent I_k induced in a pixel by a spectral irradiance $s(\lambda)$ [1].

$$f_k(\lambda) = g_L(\lambda)\, g_k(\lambda)\, g_P(\lambda) \tag{1}$$

$$I_k = \int_0^\infty f_k(\lambda)\, s(\lambda)\, d\lambda \tag{2}$$

A colour image sensor need not estimate $s(\lambda)$ at each pixel to recreate the sensation of colour implied by $s(\lambda)$ on a display device (i.e. a monitor or printer) [8]. In response to a spectral irradiance $s(\lambda)$, human perception of colour may be described fundamentally by three numbers X, Y and Z [9]. These numbers are inner products, over the visible spectrum, of $s(\lambda)$ and three basis functions $\bar{x}(\lambda)$, $\bar{y}(\lambda)$ and $\bar{z}(\lambda)$, which were standardised by the Commission Internationale de l'Eclairage (CIE) in 1931. Normally, $f_R(\lambda)$, $f_G(\lambda)$ and $f_B(\lambda)$ in (1) are designed to approximate linear combinations of $\bar{x}(\lambda)$, $\bar{y}(\lambda)$ and $\bar{z}(\lambda)$ [8]. Therefore, I_R, I_G and I_B in (2) may be modelled by linear functions of X, Y and Z, as in (3), where $\mathbf{x}$ is a vector of X, Y and Z values and $\mathbf{d}_k$ is a vector array of coefficients, called a *mask*, that relates the photocurrent I_k linearly to $\mathbf{x}$.

$$I_k = \mathbf{d}_k \bullet \mathbf{x} \tag{3}$$

Because the circuits for a colour logarithmic sensor are identical to those of a monochromatic logarithmic sensor, the same equations relate the output of the sensor to the photocurrent in a pixel. By following the analysis of Joseph and Collins for monochromatic sensors [6], the digital response y of a colour logarithmic pixel to a photocurrent I_k, given in (3), may be modelled by (4), where a, b, c and ϵ are called the *offset*, *gain*, *bias* and *error* respectively. The offset depends on threshold voltages of the circuit, the gain depends on the subthreshold slope, the bias depends on the photodiode leakage current and the error depends on random noise.

$$y = a + b \ln(c + I_k) + \epsilon \tag{4}$$

III. CALIBRATION

The model in (4) gives the response of a logarithmic pixel to irradiance focused upon it from a point in a scene. To recreate the scene on a standard display, an image must be rendered from pixel responses. Rendering accuracy depends on calibration of the parameters that relate the response of each pixel to real world stimuli. The calibration divides into two parts, one dealing with FPN and the other with colour.

A. Fixed pattern noise

FPN arises in a logarithmic image sensor, resulting in non-uniform images of uniform surfaces, when a, b, c or a combination thereof vary from pixel to pixel. This distortion is predictable and largely correctable. Joseph and Collins identify three types of FPN of interest [6]. The first involves offset variation, where only the offset varies with the pixel coordinate j in an array of N pixels, where $1 \le j \le N$. The second involves offset and gain variation and the third involves offset, gain and bias variation. The design and fabrication of a sensor may favour one of these types so all three are considered here.

To correct FPN, the varying parameters are estimated using images of uniform irradiance, preferably white in colour, taken with M different intensities [6]. Indexing these images by i, where $1 \le i \le M$, the estimated response $\hat{y}_{ij}$ of the sensor (as opposed to the actual response y_{ij}, which includes an unpredictable error component ϵ_{ij}), is given in (5)–(7) for single, double and triple variation respectively. With $k \in \{R, G, B\}$, k_j represents the pattern of overlaid colour filters.

$$\hat{y}_{ij} = a_j + b \ln\left(c + I_{ik_j}\right) \tag{5}$$

$$\hat{y}_{ij} = a_j + b_j \ln\left(c + I_{ik_j}\right) \tag{6}$$

$$\hat{y}_{ij} = a_j + b_j \ln\left(c_j + I_{ik_j}\right) \tag{7}$$

When pixels are partitioned by colour, the calibration of FPN in a colour sensor becomes the calibration of FPN in three monochromatic sensors. Following Joseph and Collins [6], parameters in (5)–(7) may be estimated by minimising three sum square errors (SSEs) in (8) between the actual responses y_{ij} and the estimated responses $\hat{y}_{ij}$ for colours $k' = R, G, B$.

$$SSE_{k'} = \sum_{i=1}^{M} \sum_{j|k_j=k'} \left(y_{ij} - \hat{y}_{ij}\right)^2 \tag{8}$$

Parameters estimated by minimising the SSEs are not unique [6]. Note that (5) and (6) are invariant under transformations (9)–(11), with b replaced by b_j in the case of (6). Similarly, (7) is invariant under transformations (9) and (11), with b and c replaced by b_j and c_j respectively, but (10) does not apply.

$$(a_j, b, c, I_{ik}) \equiv (a_j - b \ln \gamma, b, \gamma c, \gamma I_{ik}) \tag{9}$$

$$(a_j, b, c, I_{ik}) \equiv \left(a_j, \frac{b}{\gamma}, 0, (c + I_{ik})^\gamma\right) \tag{10}$$

$$(a_j, b, c, I_{ik}) \equiv (a_j, b, c - \gamma, I_{ik} + \gamma) \tag{11}$$

Parameter estimation in (5)–(7) is limited for each partition by (9)–(11) [6]. For offset variation in (5), the means of the offsets $\bar{a}_k$, the gain b and the bias c are inestimable but the deviation of the offsets from the means, denoted $\hat{a}_j$ in (12), is estimable.

$$\hat{a}_j \approx a_j - \bar{a}_{k_j} \tag{12}$$

Similarly, for offset and gain variation in (6), the means of the offsets $\bar{a}_k$, the means of the gains $\bar{b}_k$ and the bias c are inestimable. The estimated offsets and gains, denoted $\hat{a}_j$ and $\hat{b}_j$ in (13) and (14), are linear functions of the actual parameters.

$$\hat{a}_j \approx a_j - b_j \frac{\bar{a}_{k_j}}{\bar{b}_{k_j}} \tag{13}$$

$$\hat{b}_j \approx \frac{b_j}{\bar{b}_{k_j}} \tag{14}$$

For offset, gain and bias variation in (7), the means of the offsets $\bar{a}_k$ and the means of the biases $\bar{c}_k$ are inestimable. The estimated offsets, gains and biases, denoted $\hat{a}_j$, $\hat{b}_j$ and $\hat{c}_j$ in (15)–(17), are linear functions of the actual parameters.

$$\hat{a}_j \approx a_j - b_j \frac{\bar{a}_{k_j}}{\bar{b}_{k_j}} \tag{15}$$

$$\hat{b}_j \approx b_j \tag{16}$$

$$\hat{c}_j \approx e^{\frac{\bar{a}_{k_j}}{\bar{b}_{k_j}}} \left(c_j - \bar{c}_{k_j}\right) \tag{17}$$

Equation (18) estimates the standard deviation of the residual error $\hat{\sigma}_\epsilon$ for FPN calibration. The square of this measure equals the total SSE in (8) over the degrees of freedom (DOF), which is the number of constraints (i.e. MN) minus the number of parameters fitted to the same constraints (i.e. $3M+N$, $3M+2N$ and $3M+3N$ for single, double and triple variation).

$$\hat{\sigma}_\epsilon^2 = \frac{1}{DOF} \sum_{i=1}^{M} \sum_{j=1}^{N} \left(y_{ij} - \hat{y}_{ij}\right)^2 \tag{18}$$

B. Colour

Once the offset, gain and bias parameters that govern FPN are calibrated, the mask parameters in (3) need calibration to render an image taken by a colour logarithmic sensor into a standard colour space. Colour calibration of conventional linear sensors is done by imaging a colour chart with patches of known colour and using these ideal values and corresponding image data to estimate parameters of the colour model [8]. The approach given below deals with a calibration using M images of the colour chart, indexed by i, taken with different illuminant intensities to cover a wide dynamic range.

The images are segmented to locate and separate the pixels that correspond to each colour patch. So that FPN does not corrupt segmentation, the images are first corrected using the results $\hat{a}_j$, $\hat{b}_j$ and $\hat{c}_j$ of FPN calibration as with monochromatic sensors [6]. The response of each pixel in each colour patch of each image may be estimated by (19)–(21) for single, double and triple variation, where $\mathbf{x}_{ij}$ is the ideal colour vector of the j^{th} pixel with the i^{th} illuminant intensity.

$$\hat{y}_{ij} = \hat{a}_j + \bar{a}_{k_j} + b \ln\left(c + \mathbf{d}_{k_j} \bullet \mathbf{x}_{ij}\right) \tag{19}$$

$$\hat{y}_{ij} = \hat{a}_j + \hat{b}_j \bar{a}_{k_j} + \hat{b}_j \bar{b}_{k_j} \ln\left(c + \mathbf{d}_{k_j} \bullet \mathbf{x}_{ij}\right) \tag{20}$$

$$\hat{y}_{ij} = \hat{a}_j + \hat{b}_j \frac{\bar{a}_{k_j}}{\bar{b}_{k_j}} + \hat{b}_j \ln\left(e^{-\frac{\bar{a}_{k_j}}{\bar{b}_{k_j}}} \hat{c}_j + \bar{c}_{k_j} + \mathbf{d}_{k_j} \bullet \mathbf{x}_{ij}\right) \tag{21}$$

Several unknowns remain from FPN calibration in (19)–(21). These parameters may be reduced, as in (22)–(24), by combining some unknowns together with substitutions (25) and (26) (with $\bar{b}_k$ instead of b, and $\bar{c}_k$ instead of c, as appropriate).

$$\hat{y}_{ij} = \hat{a}_j + b \ln\left(c'_{k_j} + \mathbf{d}'_{k_j} \bullet \mathbf{x}_{ij}\right) \tag{22}$$

$$\hat{y}_{ij} = \hat{a}_j + \hat{b}_j \bar{b}_{k_j} \ln\left(c'_{k_j} + \mathbf{d}'_{k_j} \bullet \mathbf{x}_{ij}\right) \tag{23}$$

$$\hat{y}_{ij} = \hat{a}_j + \hat{b}_j \ln\left(\hat{c}_j + c'_{k_j} + \mathbf{d}'_{k_j} \bullet \mathbf{x}_{ij}\right) \tag{24}$$

$$c'_k = e^{\frac{\bar{a}_k}{b}} c \tag{25}$$

$$\mathbf{d}'_k = e^{\frac{\bar{a}_k}{b}} \mathbf{d}_k \tag{26}$$

The remaining parameters are estimated by minimising the SSE in (27) between the actual response y_{ij} and estimated response $\hat{y}_{ij}$ for pixels of the colour chart, given by the set $\mathcal{C}$. Minimising the SSE for any of the models in (22)–(24) requires optimisation as no analytic solution exists for all the unknowns. However, at the minimum of the SSE, b and $\bar{b}_k$ in (22) and (23) are given by (28) and (29), where l_{ij} is given in (30).

$$SSE = \sum_{i=1}^{M} \sum_{j \in \mathcal{C}} \left(y_{ij} - \hat{y}_{ij}\right)^2 \tag{27}$$

$$b = \frac{\sum_{i=1}^{M} \sum_{j \in \mathcal{C}} \left(y_{ij} - \hat{a}_j\right) l_{ij}}{\sum_{i=1}^{M} \sum_{j \in \mathcal{C}} l_{ij}^2} \tag{28}$$

$$\bar{b}_{k'} = \frac{\sum_{i=1}^{M} \sum_{j \in \mathcal{C} | k_j = k'} \left(y_{ij} - \hat{a}_j\right) \hat{b}_j l_{ij}}{\sum_{i=1}^{M} \sum_{j \in \mathcal{C} | k_j = k'} \hat{b}_j^2 l_{ij}^2} \tag{29}$$

$$l_{ij} = \ln\left(c'_{k_j} + \mathbf{d}'_{k_j} \bullet \mathbf{x}_{ij}\right) \tag{30}$$

Thus, only 12 variables that make up c'_k and $\mathbf{d}'_k$ need optimisation for models (22)–(24). A suitable optimisation algorithm is the conjugate gradients method [10]. Care must be taken to ensure that chosen parameters of c'_k and $\mathbf{d}'_k$, in either of (22)–(24), keep the argument of the logarithm positive. This can be done by making the SSE in (27) otherwise return a large value (∞ in Matlab) and ensuring that the line minimisation used by the conjugate gradients method can cope with such extremes.

Equation (31) estimates the standard deviation of the residual error $\hat{\sigma}_\epsilon$ in colour calibration. The square of this measure equals the SSE in (27) divided by the DOF, which is M times the cardinality of $\mathcal{C}$ minus the number of fitted parameters (i.e. 13, 15 and 12 for single, double and triple variation).

$$\hat{\sigma}_\epsilon^2 = \frac{1}{DOF} \sum_{i=1}^{M} \sum_{j \in \mathcal{C}} \left(y_{ij} - \hat{y}_{ij}\right)^2 \tag{31}$$

IV. RENDITION

The purpose of a colour image sensor is to provide an image of a scene that is similar to the real scene when displayed. Thus, pixel responses must be rendered into a well-defined colour space, such as CIE XYZ [9]. Denoting the offset, gain and bias parameters estimated by FPN calibration as $\hat{a}_j$, $\hat{b}_j$ and $\hat{c}_j$ and those estimated by colour calibration as $\hat{b}$ (or $\hat{b}_k$) and $\hat{c}_k$, equations (32)–(35) estimate the response $\hat{y}_j$ of a logarithmic pixel for single, double and triple variation to a stimulus $\mathbf{x}_j$.

$$\hat{y}_j = \hat{a}_j + \hat{b} \ln\left(\hat{c}_{k_j} + I'_j\right) \tag{32}$$

$$\hat{y}_j = \hat{a}_j + \hat{b}_j \hat{b}_{k_j} \ln\left(\hat{c}_{k_j} + I'_j\right) \tag{33}$$

$$\hat{y}_j = \hat{a}_j + \hat{b}_j \ln\left(\hat{c}_j + \hat{c}_{k_j} + I'_j\right) \tag{34}$$

$$I'_j = \mathbf{d}'_{k_j} \bullet \mathbf{x}_j \tag{35}$$

Rendering the response y_j into CIE XYZ space involves estimating the stimulus $\mathbf{x}_j$. First, I'_j is estimated by minimising the SSE in (36) between the actual response y_j and estimated response $\hat{y}_j$ of the sensor. Such minimisation amounts to inversion of (32)–(34), giving estimates $\hat{I}_j$ in (37)–(39).

$$SSE = \sum_{j=1}^{N} \left(y_j - \hat{y}_j\right)^2 \tag{36}$$

$$\hat{I}_j = e^{\frac{y_j - \hat{a}_j}{\hat{b}}} - \hat{c}_{k_j} \tag{37}$$

$$\hat{I}_j = e^{\frac{y_j - \hat{a}_j}{\hat{b}_j \hat{b}_{k_j}}} - \hat{c}_{k_j} \tag{38}$$

$$\hat{I}_j = e^{\frac{y_j - \hat{a}_j}{\hat{b}_j}} - \hat{c}_j - \hat{c}_{k_j} \tag{39}$$

Next, $\hat{I}_j$ is interpolated to estimate red, green and blue responses, denoted $\hat{I}_{jk}$, at each pixel j. Linear interpolation over a small neighbourhood suffices as the responses of a pixel and its neighbours are highly correlated. Due to (35), the interpolated estimates depend linearly on the stimulus $\mathbf{x}_j$. Inverting this dependence in (40), using the estimated mask $\hat{\mathbf{d}}_k$ in matrix form, gives the desired estimate, denoted $\hat{\mathbf{x}}_j$, of the stimulus.

$$\hat{\mathbf{x}}_j = \begin{pmatrix} \hat{d}_{1R} & \hat{d}_{2R} & \hat{d}_{3R} \\ \hat{d}_{1G} & \hat{d}_{2G} & \hat{d}_{3G} \\ \hat{d}_{1B} & \hat{d}_{2B} & \hat{d}_{3B} \end{pmatrix}^{-1} \begin{pmatrix} \hat{I}_{jR} \\ \hat{I}_{jG} \\ \hat{I}_{jB} \end{pmatrix} \tag{40}$$

Images in CIE XYZ space may be rendered into other spaces. For example, $\hat{\mathbf{x}}_j$ in (40) may be rendered into CIE Lab space [9]. Euclidean distances in Lab space correlate with perceptual differences. Equation (41) estimates the standard deviation of the perceptual error $\hat{\sigma}_E$ between the ideal Lab vectors $\mathbf{z}_{ij}$ and the estimated Lab vectors $\hat{\mathbf{z}}_{ij}$ for the M calibration images of the colour chart. The DOF in (41) is the same as in (31).

$$\hat{\sigma}_E^2 = \frac{1}{DOF} \sum_{i=1}^{M} \sum_{j \in \mathcal{C}} \left\| \mathbf{z}_{ij} - \hat{\mathbf{z}}_{ij} \right\|^2 \tag{41}$$

V. EXPERIMENTS

Experiments were done with a Fuga 15RGB logarithmic image sensor, which had a 512×512 pixel array (i.e. $N = 512^2$). Rather than vary the intensity of the fluorescent illuminant, neutral density filters with nominal optical densities of 0.5, 1.0, 1.5 and 2.0 were used to simulate two decades of intensity variation. Effective illuminances were measured with a light meter for each filter and for the case of no filter.

A. Calibration

A sheet of white paper made a uniform scene for FPN calibration. Five images were taken (i.e. $M = 5$) using the neutral density filters to span two decades of illuminance. Following Section III-A, the single, double and triple variation models were calibrated. The standard deviation of the residual error, given in (18), was 5.1, 2.2 and 0.6 counts for these models. Thus, triple variation represents FPN well for the Fuga 15RGB.

Next, five images were taken of a Macbeth chart, created by McCamy et al [11], which had 24 painted patches covering a wide gamut of colours. Using the neutral density filters to span two decades of illuminance, the images covered a dynamic range of 3.5 decades as the patches spanned 1.5 decades of reflectance. Following Section III-B, colour calibration was performed. On average, there were 3,839 pixels in each of the 24 patches in each of the five images. The standard deviation of the residual error, given in (31), was 6.1, 3.9 and 9.4 counts for single, double and triple variation respectively.

Figure 1 plots the standard deviation of the residual error, marked by crosses, versus illuminance for colour calibration. That triple variation performs much worse than single or double variation is surprising considering the residual error for FPN calibration is much better for triple variation. Investigation of the colour chart data reveals that, as with the white paper data, triple variation models FPN better than single or double variation. However, the dependence in (4) of the digital response y on the photocurrent I_k is unsuitable for estimating colour. A comparison of ideal colours with estimated colours suggests a model, given in (42), using the function in (43).

$$y = a + b \ln\left(c + f\left(I_k\right)\right) + \epsilon \tag{42}$$

$$f\left(I\right) = \left(\alpha + I\right)^{\beta} \tag{43}$$

Assuming α and β in (43) are constant from pixel to pixel, replacing the ideal model of (4) with the empirical model of (42) does not change the results of FPN calibration. The unknowns I_{ik} in Section III-A are replaced by the unknowns $f(I_{ik})$ with no change to offset, gain and bias estimates. However, colour calibration in Section III-B must estimate α and β by including them in the conjugate gradients optimisation. As they modify the partial derivatives of the SSE in (27), these parameters affect the estimation of other parameters. Furthermore, the DOF in (31) and (41) must account for estimation of α and β.

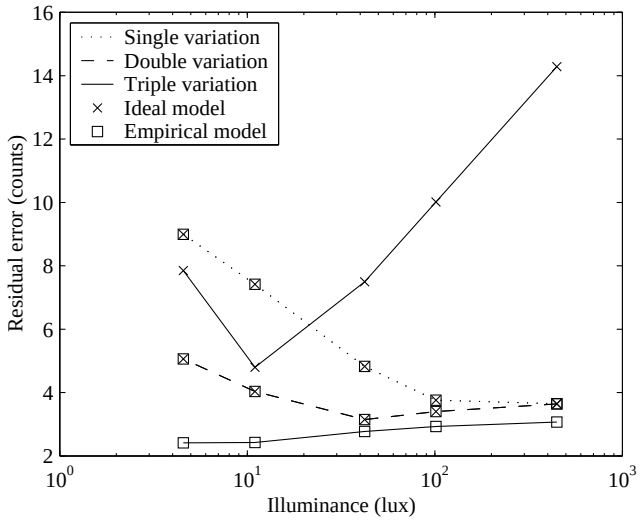

Fig. 1. Residual error of colour calibration versus illuminant intensity for the single, double and triple variation (ideal and empirical) models.

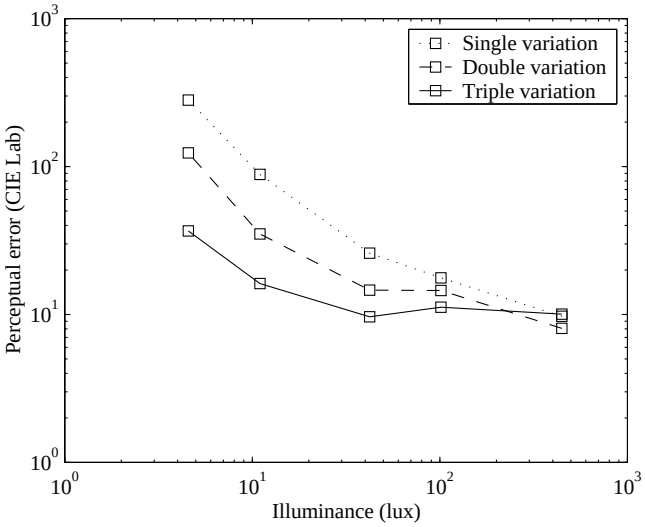

Fig. 2. Perceptual error of rendering a Macbeth chart versus illuminant intensity for the single, double and triple variation (empirical) models.

Repeating colour calibration with the empirical model results in a standard deviation of the residual error equal to 6.1, 3.9 and 2.7 counts for single, double and triple variation. Figure 1 plots the standard deviation of the residual error, marked by squares, versus illuminance. Colour calibration with the empirical model improves over the ideal model substantially for triple variation but negligibly for single and double variation. The latter may be unable to discriminate I_k in (4) from $f(I_k)$ in (42) due to a higher residual error from FPN calibration.

The empirical model for triple variation shows a residual error for colour calibration that is nearly flat across 3.5 decades of dynamic range (each point in Figure 1 comprises 1.5 decades). However, with the ideal or empirical model, the residual error increases with decreasing illuminance for single and double variation. This dependence suggests that bias variation, not considered by single and double variation, degrades colour calibration mainly in dim lighting. For triple variation, the slight increase in error with increasing illuminance may be because the neutral density filters, used in taking the dimmer four images, did not really have flat spectral responses and thus modified the colour of transmitted light in addition to the intensity.

B. Rendition

After FPN and colour calibration, images taken by the Fuga 15RGB may be rendered into a standard colour space such as CIE XYZ or CIE Lab, following Section IV for the ideal model. For the empirical model, the rendering must include an inversion of (43). Using the empirical model, the standard deviation of the perceptual error, given in (41), between the ideal colour chart and rendered images of the chart was 133, 58 and 20 for single, double and triple variation respectively. Figure 2 plots the standard deviation of the perceptual error versus illuminance. The figure shows how close the colours of the ideal chart match those of the rendered chart from the perspective of a standard observer (as defined by the CIE).

TABLE I

PERCEPTUAL ERROR OF CONVENTIONAL DIGITAL CAMERAS BETWEEN IDEAL AND ACTUAL IMAGES OF A MACBETH CHART.

Digital camera	Error (CIE Lab)
Kodak DCS 265	13
Nikon Coolpix 950	12
Olympus Camedia C-2000 Zoom	16
Canon Powershot Pro 70	17
Ricoh RDC 4200	13
Agfa ePhoto CL 50	15
Fuji MX 2700	15

To put the performance of colour rendition with the Fuga 15RGB in perspective, the perceptual error between an image of the ideal Macbeth chart and images of the chart rendered by conventional digital cameras were calculated from an article by McNamee [12]. The images were scanned with an HP Scanjet 5300C and converted into CIE Lab space. Table I lists the standard deviation of the perceptual error between pixels of the ideal chart and corresponding pixels of each camera's image.

Comparing Table I to Figure 2 for single and double variation, colour rendition is better with conventional cameras than with the Fuga 15RGB. For triple variation, colour rendition of the Fuga 15RGB is comparable to conventional cameras except in dim lighting. Excluding the dimmest image, taken with five lux of illuminance, the standard deviation of the perceptual er-

ror is 12 with the Fuga 15RGB for triple variation. This result is comparable to the overall standard deviation in Table I, which equals 15. As the Macbeth chart spans 1.5 decades of reflectance and the Fuga 15RGB images, excluding the dimmest, span 1.5 decades of illuminance, colour rendition of the logarithmic sensor, tested over three decades of dynamic range, competes with colour rendition of conventional cameras, tested over 1.5 decades (McNamee used only one illuminance [12]).

The perceptual error in Figure 2 increases with decreasing illuminance even for triple variation, which has a residual error in Figure 1 that decreases with decreasing illuminance. In dim lighting, the bias c (and α) dominates the logarithm in (42) and makes the stimulus $\mathbf{x}$ in (3) difficult to estimate. In other words, photodiode leakage currents reduce the sensitivity of pixels to small photocurrents so that the random noise ϵ in (42) has a greater effect on the response than the stimulus. Decreasing the leakage current, increasing the photocurrent or reducing the random noise should lessen this degradation. Decreasing the leakage current would also reduce bias variation and improve the relative performance of double variation.

VI. CONCLUSION

Logarithmic CMOS image sensors have a capability to capture scenes bearing a high dynamic range of illuminance and reflectance in a manner that roughly approximates human perception [2]. Permitting high frame rates, they are an attractive technology for motion tracking in outdoor environments [4], [5]. However, research on colour logarithmic sensors has been limited by a lack of theory and results on modelling, calibration and rendition of sensor responses in terms of a standard colour space. This paper begins to address these problems.

A model for the response of a colour logarithmic sensor to spectral irradiance was constructed by combining the colour model of conventional linear sensors [8] with the monochromatic model of logarithmic sensors [6]. Thus, the digital response y of a logarithmic pixel to a colour stimulus $\mathbf{x}$, given in CIE XYZ space [9], is modelled by $y = a + b\ln(c + \mathbf{d}_k \bullet \mathbf{x}) + \epsilon$ where a, b, c, $\mathbf{d}_k$ and ϵ are called the *offset*, *gain*, *bias*, *mask* and *error* respectively, with k identifying if the pixel is selective to the red, green or blue regions of the spectrum.

Pixel-to-pixel variation of the offset, gain, bias or a combination thereof leads to fixed pattern noise (FPN), which distorts an image in a repeatable and predictable way, most visible with uniform surfaces [6]. Calibration of the image sensor involves estimation of the model parameters. First, the varying parameters are estimated by partitioning pixels by colour sensitivity and applying the method of monochromatic FPN calibration to each partition [6]. Second, the mask and other variables remaining from FPN calibration are estimated using images of a reference colour chart. Calibrated models may be used to render an image taken with the sensor into CIE XYZ space and then into other useful spaces, such as CIE Lab [9].

Using neutral density filters to simulate varying illuminance, experiments were performed with a Fuga 15RGB sensor. A pixel-to-pixel variation of offset, gain and bias modelled FPN well, with a residual error of 0.6 counts for FPN calibration of white paper. Colour calibration of a Macbeth chart [11] showed that the ideal model did not match the sensor response. An empirical model $y = a + b\ln(c + (\alpha + \mathbf{d}_k \bullet \mathbf{x})^\beta) + \epsilon$ worked well, with a residual error of 2.7 counts for colour calibration. The perceptual error with this model was 12, in CIE Lab space, over three decades of dynamic range, comparable to conventional digital cameras over 1.5 decades. The perceptual error increased quickly below five lux of illuminance, possibly because leakage currents reduced the sensitivity of pixels.

Instead of focusing on analogue methods to compensate for offset variation, research in logarithmic sensors should aim to minimise bias variation so that offset or offset and gain variation suffices to model FPN, and to minimise average bias, so that colour rendition in dim lighting improves. As the mask depends on spectral responses of photodiodes and overlaid filters and does not seem to vary across pixels, it may be estimated once for a process (a common practice with conventional linear cameras [8]) rather than for every sensor. Furthermore, the effect of temperature on pixel responses needs examination.

References

[1] Tarek Lulé, Stephan Benthien, Holger Keller, Frank Mütze, Peter Rieve, Konstantin Seibel, Michael Sommer, and Markus Böhm, "Sensitivity of CMOS Based Imagers and Scaling Perspectives," *IEEE Transactions on Electron Devices*, vol. 47, no. 11, pp. 2110–22, Nov. 2000.

[2] Orly Yadid-Pecht, "Wide-dynamic-range sensors," *Optical Engineering*, vol. 38, no. 10, pp. 1650–60, Oct. 1999.

[3] Robert M. Boynton, *Human Color Vision*, University of California, San Diego, 1979.

[4] B. Hoefflinger, H.-G. Graf, U. Seger, and A. Siggelkow, "Imager for Robust High-Speed Vision," in *Proceedings for the Dedicated Conference on Robotics, Motion and Machine Vision in the Automotive Industries*, 1995, pp. 289–93, 28th International Symposium on Automotive Technology and Automation.

[5] Muahel Tabet, Nick Tu, and Richard Hornsey, "Modeling and characterization of logarithmic complementary metal-oxide-semiconductor active pixel sensors," *Journal of Vacuum Science & Technology A*, vol. 18, no. 3, pp. 1006–9, May–June 2000.

[6] Dileepan Joseph and Steve Collins, "Modelling, calibration and correction of nonlinear illumination-dependent fixed pattern noise in logarithmic CMOS image sensors," in *Proceedings of the 18th IEEE Instrumentation and Measurement Technology Conference*, 2001, vol. 2, pp. 1296–1301, Rediscovering Measurement in the Age of Informatics.

[7] Bart Dierickx, Danny Scheffer, Guy Meynants, Werner Ogiers, and Jan Vlummens, "Random addressable active pixel image sensors," in *Proceedings of the SPIE*, 1996, vol. 2950, pp. 2–7, Advanced Focal Plane Arrays and Electronic Cameras.

[8] Arch C. Luther, *Video Camera Technology*, Artech House, Boston, 1998.

[9] Asim Kumar Roy Choudhury, *Modern Concepts of Colour and Appearance*, Science Publishers, Enfield, 2000.

[10] Christopher M. Bishop, *Neural Networks for Pattern Recognition*, Oxford University Press, Oxford, 1995.

[11] C. S. McCamy, H. Marcus, and J. G. Davidson, "A Color-Rendition Chart," *Journal of Applied Photographic Engineering*, vol. 2, no. 3, pp. 95–99, Summer 1976.

[12] Mike McNamee, "A Snapshot in Time," *Digital Photographer*, vol. 13, pp. 32–38, July 1999.